1-1-2011

A Comprehensive Model of a Miniature-Scale Linear Compressor for Electronics Cooling

Craig R. Bradshaw
Purdue University - Main Campus, cbradsha@purdue.edu

Eckhard A. Groll
Purdue University - Main Campus, groll@purdue.edu

Suresh V. Garimella
Purdue University, sureshg@purdue.edu

Bradshaw, Craig R.; Groll, Eckhard A.; and Garimella, Suresh V., "A Comprehensive Model of a Miniature-Scale Linear Compressor for Electronics Cooling" (2011). *Publications of the Ray W. Herrick Laboratories.* Paper 1.
http://docs.lib.purdue.edu/herrick/1

A Comprehensive Model of a Miniature-Scale Linear Compressor for Electronics Cooling

Craig R. Bradshaw[a,b,1], Eckhard A. Groll[a,b], Suresh V. Garimella[b]

[a]*Herrick Laboratories, Purdue University, West Lafayette, IN 47907*
[b]*Cooling Technologies Research Center, Purdue University, West Lafayette, IN 47907*

Abstract

A comprehensive model of a miniature-scale linear compressor for electronics cooling is presented. Linear compressors are appealing for refrigeration applications in electronics cooling. A small number of moving components translates to less theoretical frictional losses and the possibility that this technology could scale to smaller physical sizes better than conventional compressors. The model developed here incorporates all of the major components of the linear compressor including dynamics associated with the piston motion. The results of the compressor model were validated using experimental data from a prototype linear compressor. The prototype compressor has an overall displacement of approximately $3cm^3$, an average stroke of 0.6 cm. The prototype compressor was custom built for this work and utilizes custom parts with the exception of the mechanical springs and the linear motor. The model results showed good agreement when validated against the experimental results. The piston stroke is predicted within 1.3% MAE. The volumetric and overall isentropic efficiencies are predicted within 24% and 31%, MAE respectively.

Keywords: linear compressor, compressor model, electronics cooling, miniature compressor

[1]Corresponding Author, cbradsha@purdue.edu

Nomenclature

A area $[m^2]$

C_D drag coefficient for flow past reed valve $[-]$

C_v specific heat capacity at constant volume $[J\,kg^{-1}\,K^{-1}]$

D diameter $[m]$

E total energy in the control volume $[kW]$

F_{drive} driving force from linear motor $[N]$

J_{CG} rotational moment of inertia for the piston about the CG $[kg\,m]$

M moving mass $[kg]$

MAE Mean absolute error $[-]$

P pressure of gas $[kPa]$

P_{high} higher pressure $[kPa]$

P_{low} lower pressure $[kPa]$

R_{amb} thermal resistance between the compressor shell and ambient $[W\,K^{-1}]$

Re Reynolds number$[-]$

T temperature of gas$[K]$

V volume of control volume $[m^3]$

W work $[J]$

$\dot{Q}$ total heat transfer into the control volume $[kW]$

$\dot{W}$ total work on the control volume $[kW]$

$\dot{m}$ mass flow rate $[kg\ s^{-1}]$

$\mathbf{V}$ gas velocity $[m\ s^{-1}]$

$\mathbf{f}$ dry friction coefficient between piston and cylinder $[-]$

$\mathbf{k}$ thermal conductivity $[Wm^{-1}K^{-1}]$

c_{eff} effective damping of piston $[N\ s\ m^{-1}]$

f resonant frequency of piston operation $[Hz]$

g leakage gap width $[m]$

h specific enthalpy $[kJ\ kg^{-1}]$

k stiffness or spring rate $[N\ m^{-1}]$

q heat flux $[Wm^{-2}]$

t time $[sec]$

u internal energy $[kJ\ kg^{-1}]$

v specific volume of gas $[m^3\ kg^{-1}]$

x displacement $[m]$

Greek letter

α thermal diffusivity $[m^2 s^{-1}]$

ϵ eccentricity of spring force $[m]$

η efficiency $[-]$

γ heat capacity ratio $[-]$

ω_d damped natural frequency $[rad\ sec^{-1}]$

ρ density of gas $[kg\,m^{-3}]$

θ rotational angle of piston $[rad]$

Subscripts

amb ambient

cv control volume

$discharge$ gas discharged from compression chamber

exp experimental value

gas quantity resulting from gas

in into control volume

$leak$ leakage

$mech$ mechanical

o, is overall isentropic

out out of control volume

p piston

$port$ valve port opening

$shell$ compressor shell

$suction$ suction gas

tr transitional

v constant volume process

$valve$ reed valve

vol volumetric

1. Introduction

Miniature refrigeration systems offer distinct advantages for use in electronics cooling relative to other technologies. Only refrigeration offers the ability to cool components below the ambient temperature. The reliability and performance of semi-conductor devices is improved when operating at lower temperatures. Because vapor compression utilizes two-phase heat transfer in the evaporator, it is possible to maintain spatially uniform chip temperatures. The major concerns involving refrigeration systems are their cost and reliability, as well as miniaturization of the different components.

Trutassanawin et al. (2006) reviewed the available technologies for vapor compression systems in electronics cooling. Several prototype systems were discussed but there appeared to be no commercially viable solutions which are complete miniature systems. Chiriac and Chiriac (2008) concurred with this assessment in a recent review. Other investigations into refrigeration technology have led to the development of system prototypes (Mongia et al., 2006) and system-level models such as ones by Heydari (2002) and Possamai et al. (2008). However, it has been reported that the overall performance and size of these systems is still not at a level that is desired for desktop and portable electronic systems (Cremaschi et al., 2007). In particular the compressor is a critical component which can greatly affect the overall size and performance of the refrigeration system, as shown by Trutassanawin et al. (2006).

In electronics cooling applications, an atypical challenge for refrigeration systems is the relatively small temperature lift for cycle operation. The temperature lift is limited on the high-side by the environmental conditions and on the low-side by the desire to eliminate possible water vapor condensation from the ambient within the electronic package. Typically, this leads to a system with a small pressure ratio, as shown in Figure 1, which displays a typical refrigeration cycle for electronics cooling using R-134a as the working fluid. The small pressure ratio leads to poor performance for currently available small-scale compressors, which are designed for refrigerator applications with a significantly larger pressure ratio. Some past studies using currently available technology have operated the compressors at a

larger pressure ratio, and instead, developed solutions to handle moisture condensation by operating the evaporator and chip assembly in heavily insulated volumes (Heydari, 2002). The disadvantage of this option is a further increase in the cost of the cooling system.

A linear compressor is appealing for electronics cooling applications because it offers several potential advantages over traditional compressor technology. A linear compressor is a positive displacement compressor, similar to a reciprocating compressor. However, a linear compressor does not have a crank mechanism to drive the piston. Instead the piston is driven directly by a linear motor, as seen in Figure 2. The omission of the crank mechanism significantly reduces the frictional losses associated with conventional reciprocating compressors. It also allows oil-free operation which is a significant advantage with respect to the heat transfer performance of the condenser and evaporator in the system.

In addition, a linear compressor is designed as a resonantly operated device. This means that mechanical springs are used to tune the device to operate at a resonant frequency. Operation at a resonant frequency allows a desirable reduction in size of the motor.

Early investigations of a linear compressor were conducted by Cadman and Cohen (1969a,b) for traditional refrigeration systems. Cadman and Cohen observed that the free piston operation of this device created some peculiar effects such as piston drift, which posed a challenge to modeling efforts and limited the practical application such devices. Pollak et al. (1979) investigated one-dimensional, nonlinear dynamics of the piston and electrical systems and confirmed such confounding effects.

Van der Walt and Unger (1994) assessed the state of the art in linear compressor technology. Unger and Novotny (2002) and Unger (1998) developed several linear compressor prototypes and performed a feasibility study which showed the potential for linear compressors in cryogenic and miniature systems. There have also been studies on the unique differences in the performance of linear compressors compared to conventional reciprocating compressors (Lee et al., 2001, 2004). Recently, Possamai et al. (2008) developed a prototype refrigeration system for a laptop cooling application which utilized a linear compressor. Another recent study on linear compressors investigated the sensitivity of the device to changes

in operating frequency (Kim et al., 2009). This study utilized a single degree of freedom vibration model coupled to an electrodynamic motor model as was done by Pollak et al. (1979).

Past models of linear compressors have often employed linearizing assumptions or were restricted to a single degree of freedom in their analysis. Such analyses have either used a greatly simplified representation of device operation or have focused on specific components of the overall system. The present work develops a comprehensive compressor model which incorporates all of the major dynamics and nonlinearities as well as a second degree of freedom in the piston motion. In addition, the model predictions are validated using experimental data from a prototype linear compressor.

2. Model Formulation

The major components of the linear compressor model are described in this section. The comprehensive compressor model consists of a solution to two compression process equations that provide the temperature and density, and thus fix the state within each control volume. These equations require inputs from the five sub-models representing the valve flows, leakage flows, motor losses, heat transfer from the cylinder, and piston dynamics. The compression cycle is discretized and an initial guess of temperature and density is made within each control volume. The compression process equations are then used to step through a compression cycle using the numerical techniques described in Section 2.7. Comprehensive compressor models of this nature have been developed for other compressor types (Chen et al., 2002a,b, Kim and Groll, 2007, Mathison et al., 2008).

2.1. Compression Process Equations

The compression process is modeled using mass and energy conservation over a control volume. In order to determine the state of the working fluid in the compression chamber at any point during the compression process, it is necessary to determine two independent fluid properties to fix its state. In this analysis the compressor is split into two control volumes as illustrated in Figure 2. The first is the compression chamber for the compressor, while the

7

second consists of the remaining volume within the compressor. The compression process equations are solved for each control volume at a particular time step and coupled through the leakage, vibration, and heat transfer sub-models.

The fluid is assumed to be superheated throughout the entire compression process. The equation of state for the chosen working fluid, R-134a, is written in terms of temperature and density (Tillner-Roth and Baehr, 1994); the compression process equations are therefore cast in terms of these two variables. The conservation of energy for a general control volume can be written as follows:

$$\frac{dE_{cv}}{dt} = \dot{Q} + \dot{W} + \sum_{in} \dot{m}_{in}h_{in} - \sum_{out} \dot{m}_{out}h_{out} \tag{1}$$

Assuming that the fluid in the control volume is well mixed, h_{out} becomes h_{cv} and will be denoted as such in the remainder of this work. With a further assumption that the changes in kinetic and potential energies are negligible, the left-hand side of Equation (1) can be expanded in terms of changes in internal energy and mass. The following thermodynamic relations also hold for the gas in the cylinder.

$$du = C_v dT + \left[T \left(\frac{\partial P}{\partial T} \right)_v - P \right] dv \tag{2}$$

Using the relationship in Equation (2) and the definition of enthalpy, the left-hand side of Equation (1) can be written as follows:

$$\frac{dE_{cv}}{dt} = m_{cv} \left(C_v \frac{dT}{dt} + \left[T \left(\frac{\partial P}{\partial T} \right)_v - P \right] \frac{dv_{cv}}{dt} \right) + (h - Pv) \frac{dm_{cv}}{dt} \tag{3}$$

The work term from Equation (1) can be re-written as boundary work done by the piston. In order to eliminate pressure from Equation (1) the pressure in the cylinder is expressed as follows:

$$P_{cv} = T_{cv} \left(\frac{\partial P}{\partial T} \right)_v \tag{4}$$

By combining these relations:

$$m_{cv}C_v\frac{dT}{dt} + T\left(\frac{\partial P}{\partial T}\right)_v\left[\frac{dV}{dt} - \frac{1}{\rho}\frac{dm_{cv}}{dt}\right] + h_{cv}\frac{dm_{cv}}{dt} = \dot{Q} + \sum \dot{m}h_{in} - \sum \dot{m}h_{cv} \qquad (5)$$

in which only temperature is the independent variable. The other independent fluid property is density, which is computed as:

$$\frac{dm_{cv}}{dt} = \frac{d(\rho V)}{dt} = \rho\frac{dV}{dt} + V\frac{d\rho}{dt} \qquad (6)$$

The change in mass in the cylinder can then be written as:

$$\frac{dm_{cv}}{dt} = \frac{dm_{in}}{dt} + \frac{dm_{leak,in}}{dt} - \frac{dm_{out}}{dt} - \frac{dm_{leak,out}}{dt} \qquad (7)$$

Equations (5) - (7) can now be solved simultaneously for the temperature and density in the two control volumes. Due to the nonlinear nature of these equations, a numerical solution approach is adopted. A number of inputs to this solution must still be determined from various sub-models as will be discussed below.

2.2. Valve Model

Reed valves are used in the present work as is typical for reciprocating compressors. These valves are essentially cantilevered beams which are displaced when a differential pressure is imposed across them. To ensure that pumping, as opposed to back flow, of the gas occurs, two valves are used with limited ranges of operation. The valve body is constructed to only allow valve motion in the direction of desired flow for each valve; this ensures that pumping occurs and can be seen in Figure 3.

Valve analysis is split into two modes of operation depending on the location of the valve reed, similar to the analysis of Kim and Groll (2007). Early in its deflection the stagnation pressure driving the valve reed is assumed equal to the high side pressure. As the valve opens further, this assumption becomes less valid, as the movement of the valve is now dominated by the movement of fluid past the valve and the stagnation pressure becomes equal to the low-side pressure. These two modes of operation are referred to as the pressure-dominant

9

and mass-flux-dominant modes, respectively, with free-body diagrams as shown in Figure 4. The port area is a fixed quantity and represents the opening that fluid travels through in the valve body. The valve area is an effective area, taken as a circular area based on the width of each valve reed.

For each mode of operation an equation can be written based on the free-body diagrams shown in Figure 4. Summing the forces in the direction of displacement, the equation of motion for the pressure-dominated and mass flux-dominated modes may be expressed as:

$$M_{valve}\ddot{x}_{valve} + \frac{1}{2}C_D\rho A_{valve}\dot{x}_{valve}^2 + k_{valve}x_{valve} = (P_{high} - P_{low})A_{valve} + \frac{1}{2}C_D\rho\mathbf{V}^2 A_{valve} \quad (8)$$

$$M_{valve}\ddot{x}_{valve} + \left(\frac{1}{2}C_D\rho A_{port} + \rho A_{valve}\right)\dot{x}_{valve}^2 + k_{valve}x_{valve} = \frac{1}{2}C_D\rho\mathbf{V}^2 A_{valve} + \rho\mathbf{V}A_{port} \quad (9)$$

These second-order, nonlinear equations can be solved for the position of the reeds at each time step throughout the compression process. The valve geometry, shown in Figure 3, can be used to determine the required valve and port areas and the density is calculated from the compression process equations. The gas velocity is calculated assuming an isentropic, compressible flow across the valve. The mass and stiffness of the reeds can be calculated by assuming that each reed behaves as an Euler beam. The stiffness is calculated by dividing an arbitrary applied force by the deflection it produces. The effective mass is then found by dividing the total valve mass by a factor of three, as in the case of the effective mass of a spring (Rao, 2004).

At a certain valve lift, which is the ratio of the valve port opening diameter to the reed valve diameter, these two analyses provide the same mass flow rate. This valve lift is known as the transitional valve lift because below this value the pressure-dominated model is used and above the mass-flux dominated model is used. When the valve lift is equal to the transitional lift value the pressure-dominant model is used. The transitional valve lift is expressed as:

10

$$x_{tr} = \frac{D_{port}^2}{4D_{valve}} \tag{10}$$

2.3. Leakage Model

The leakage model only focuses on leakage past the piston. The only other leakage paths, those past the reed valves, are ignored since they are negligibly small compared to the leakage past the piston (Kim and Groll, 2007). The piston leakage is modeled as an incompressible Couette-Poiseuille flow driven by the pressure difference across the piston and the movement of the piston. This assumption is valid because the flow Mach number in the simulations is found to be between 0.1 and 0.3 at the representative conditions in the experiment.

The leakage mass flow rate is calculated using the average leakage velocity obtained by integrating the velocity profile as:

$$\dot{m} = \rho \bar{\mathbf{V}}_{leak} A_{leak} = \rho A_{leak} \frac{1}{g} \int_0^g \mathbf{V}_{leak}(y) dy = \frac{\dot{x}_p}{2} + \frac{g^2}{4\mu}\left(\frac{-dP}{dx}\right) + \frac{g^3}{6\mu}\left(\frac{dP}{dx}\right) \tag{11}$$

2.4. Heat Transfer Model

The instantaneous heat transfer from each of the control volumes is calculated using the empirical approach of Fagotti and Prata (1998).

$$Nu = \frac{q_{cv}D}{\mathbf{k}[T_{gas} - T_{shell}]} = 0.28Re^{0.65} + 0.25L\frac{T_{shell}}{T_{gas} - T_{shell}} \tag{12}$$

where:

$$L = \frac{\gamma - 1}{V}\frac{dV}{dt}\sqrt{\frac{D^3}{\alpha\dot{x}_p}} \tag{13}$$

By integrating these instantaneous heat transfer rates over the entire cycle, the total heat transfer from each of the two control volumes is calculated for use in the overall energy balance.

2.5. Vibration Model

A linear compressor is a free-piston device for which the stroke is not fixed by a crank mechanism but is instead determined by chosen geometry, the linear motor, and the mechanical springs used. The piston dynamics are modeled using a free body diagram of the piston assembly as shown in Figure 5.

Both the desired linear motion of the piston as well as its undesirable rotation due to eccentricity in the mechanical springs are considered. Any eccentricity causes a perpendicular reactionary load from the mechanical spring as it is compressed, since the spring cannot react to a load along its entire circumference. Thus, the effective load acts at a point offset from the center of mass of the piston. In a traditional compression spring as used in the prototype fabricated for this work, this point is assumed to be along the circumference of the spring where the edge of the spring contacts the piston assembly.

The linear motion of the piston as well as its rotation, are modeled as a two-degree of freedom vibration system. By assuming that the piston is a rigid body and the motions in the y and z directions as well as the rotation are small, the following equations describe the motion of the piston:

$$M\ddot{x}_p + c_{eff}\dot{x}_p + (k_{gas} + k_{mech})\,x_p = k_{mech}\epsilon\theta + F_{drive} \tag{14}$$

$$J_{CG}\ddot{\theta} + k_{mech}\epsilon^2\theta = k_{mech}\epsilon x_p \tag{15}$$

In addition, it is assumed that the driving force and the reactionary forces from the compression chamber are applied directly through the center of mass of the piston.

The driving force, F_{drive}, is the sinusoidal force applied from the motor. The power transmitted to the piston is calculated by assuming an efficiency for the motor. The stiffness associated with the gas, k_{gas}, is determined by linearizing the force generated by the gas over an entire compression cycle. This gas force is then divided by the stroke of the compressor which yields an effective spring rate of the gas in the compression chamber.

$$k_{gas} = \frac{(P_{discharge} - P_{suction})A_p}{x_p} \tag{16}$$

This is similar to the approach adopted by Cadman and Cohen (1969a); however, in the current work k_{gas} is updated as the guessed value of x_p changes.

The effective damping term is made up of two components: a frictional term and the boundary work performed on the gas (Pollak et al., 1979). Both components are computed from an integration of the energy dissipated over a cycle. The effective damping term is then calculated from summing the contributions described above.

$$c_{eff} = \frac{E_{cycle}}{\omega_d x_p \pi} = \frac{W_{gas}}{\omega_d x_p \pi} + \frac{W_{friction}}{\omega_d x_p \pi} \tag{17}$$

The work done on the gas is calculated by integrating the boundary work expression over the entire compression process (i.e. integrating pressure over volume). By assuming polytropic compression and expansion processes, the following expression is developed (Moran and Shapiro, 2004)

$$W_{gas} = \frac{\gamma P_{suction} V}{\gamma - 1} \left[\left(\frac{P_{discharge}}{P_{suction}} \right) - 1 \right] \tag{18}$$

where the polytropic exponent was assumed constant with a value of 1.239. The work done by friction is calculated from (Rao, 2004).

$$W_{friction} = 4\mathbf{f}Nx \tag{19}$$

2.6. Overall Energy Balance

To ensure that all of the compressor components satisfy an energy balance, a thermal network is constructed to account for heat transfer from the compression chamber (Chen et al., 2002a, Kim and Groll, 2007, Mathison et al., 2008). The energy balance for the compressor assumes that the heat transfer between the two control volumes is negligible and that the heat only flows to the compressor shell. A lumped-mass thermal network can then be constructed consisting of a single lumped mass to represent the compressor

shell with two heat inputs and one heat output to the ambient. The heat output path is calculated using a forced convection correlation for flow over a cylinder to determine the thermal resistance between the compressor shell and the ambient (Hilpert, 1933). The thermal network elements are also shown in Figure 2. This network adds the following relation which is solved simultaneously with the compression process equations.

$$\frac{T_{shell} - T_{amb}}{R_{amb}} = \dot{Q}_{cv1} + \dot{Q}_{cv2} \tag{20}$$

2.7. Solution Approach

The model developed above for the linear compressor consists of two non-linear first-order differential equations for the compression process and one non-linear equation from the energy balance. An explicit closed-form solution is not available, and the equations are instead solved numerically. The compression process is discretized into small time steps and each equation is solved using a fourth-order Runge-Kutta method.

The order in which the model steps through the series of equations is shown in Figure 6. The key input guesses to the model are the compressor inlet pressure and temperature, and the desired discharge pressure. For each time step, the model sequentially steps through each sub-model and calculates the solution inputs for the next time step. Once each sub-model has been called the overall compression process solver is called which solves Equations (5) to (7) and calculates the internal state in the compressor. When the model has iterated through an entire compression cycle Equation (20) is solved for T_{shell}. When the changes in temperature and density in each of the two control volumes as well as the change in T_{shell} is less than 0.01%, a converged solution is available. The initial conditions in both control volumes were set to the inlet conditions for each operating condition that was tested. The number of iterations required for convergence varied between approximately 20 and 150 depending on operating conditions.

3. Experiments

No linear compressors are commercially available in the capacity and pressure ranges desired for electronics cooling. Therefore, a prototype compressor was custom-designed and built for the purpose of conducting experiments that could serve to validate the model developed in this work. The compressor was built using a moving-magnet type linear motor (H2W Tech). The housings, piston, and valve assembly were built in-house. A cross-sectional view of the prototype compressor is shown in Figure 7, with key dimensions given in Table 1.

The prototype linear compressor was tested on a compressor load stand specifically built for testing miniature-scale compressors. The compressor load stand is based on a hot-gas bypass design; a schematic is shown in Figure 8. This type of load stand has been used successfully in previous studies to conduct performance tests compressors (Sathe et al., 2008, Hubacher et al., 2002). The load stand cycle state points are shown in a pressure enthalpy diagram in Figure 9. The compressor operates between state points 1 and 2. From state point 2, the gas is expanded across a set of valves to an intermediate pressure at state point 3. The flow from state point 3 is divided into two flow paths. One path runs through the condenser and is cooled to a saturated liquid at state point 4. It is then isenthalpically expanded to the compressor suction pressure at state point 5. The hot-gas bypass flow is expanded from the intermediate pressure to the compressor suction pressure at state point 6. The flows at state points 5 and 6 are mixed to provide the compressor suction state at state point 1. By controlling the ratio of these two flows the inlet pressure and temperature can be controlled. The discharge pressure of the compressor is controlled by adjusting the valve between state points 2 and 3.

The compressor was tested under a range of operating conditions, which simulate an electronics cooling application. At each specific set of compressor inlet conditions, the compressor was operated until a steady state condition was achieved, at which point data was collected. This process was then repeated for subsequent compressor inlet conditions which are tabulated in Table 2. It is noted that the performance testing of a linear compressor

15

is significantly different from that of conventional positive displacement compressors. During the performance testing of conventional compressors, the stroke and frequency of the piston are naturally held constant due to the kinematics of the device. However, a linear compressor requires that the frequency be adjusted to maintain operation at resonance. The power input and operating frequency are varied in these tests so as to maintain similar stroke values throughout the testing. The state points achieved in the experiments are summarized in Table 2.

The volumetric efficiency shown in Table 2 is defined as follows:

$$\eta_{vol} = \frac{\dot{m}_{exp}}{\rho_{suction} x_p f_{res} A_p} \tag{21}$$

This definition accounts for volumetric losses as well as a dependence on the piston dynamics. The overall isentropic efficiency of the device, also listed in Table 2, is defined as follows:

$$\eta_{o,is} = \frac{h_{2,s} - h_1}{\dot{W}} \tag{22}$$

This definition accounts for all the losses, and as a result, is used as an overall benchmark for compressor performance.

3.1. Experimental Uncertainty

A variety of measurements were obtained in the experiments including temperature and pressure at the suction and discharge ports, mass flow rate of refrigerant, piston stroke, frequency, and input power. The measurements of pressure, temperature, and stroke have absolute uncertainties of 4.6 kPa, 0.5 C, and 25.40 μm, respectively. The Coriolis mass flow meter has relative uncertainty values between 0.350 and 1.25 %, depending on the quantity of mass flow measured. The frequency and input power have absolute uncertainty values which varied from 2.07 x 10^{-4} to 5.10 x $10^{-4} Hz$ and 0.188 and 0.532 W, respectively which are calculated using a 99.95% confidence interval. The uncertainty in the reported efficiency values is calculated using an uncertainty propagation analysis (Fox et al., 2004). The volumetric and overall isentropic efficiencies have absolute uncertainty value ranges of 1.07 x 10^{-3} to 2.29 x 10^{-3} and 1.05 x 10^{-3} to 1.90 x 10^{-3}, respectively.

4. Validation of Model Predictions

The experimental results are compared to the predictions from the model. The model performance is quite sensitive to several parameters: the leakage gap between the piston and cylinder, g, the eccentricity of the piston, ϵ, the dry friction coefficient, $\mathbf{f}$, and the linear motor efficiency, η_{motor}. Since these parameters are difficult to measure, best estimates were used and adjusted within reasonable ranges to provide the best fit with the experimental data. The leakage gap was chosen based on the design dimensions to be in the range of 0.1 to $0.4mm$. The initial guess of eccentricity was set to the radius of the compression spring used in the prototype compressor, which took values in the range of 9.2 to $11.4mm$. The dry friction coefficient was varied between 0.2 and 0.4. The motor efficiency was estimated based on the measured heat loss from the prototype compressor and was varied between 40% and 50%. These parameter values are summarized in Table 1.

The parameters in Table 1 along with experimental values for the suction and discharge pressure, suction temperature, frequency, and input power (Table 2) were used as inputs to the model. Figures 10 to 13 show the major model predictions compared with the experimental results for piston stroke, mass flow rate, volumetric efficiency, and overall isentropic efficiency, respectively. The model predicts the stroke of the linear compressor within 1.3% MAE as shown in Figure 10. The predicted mass flow rates are shown in Figure 11 and agree with the measured values to within 20% MAE. The predicted volumetric efficiency shows a similar behavior to the mass flow rate, predicting the experimental results to within 24% MAE, as shown in Figure 12. In the performance testing of conventional compressors the volumetric efficiency is simply a dimensionless mass flow rate. However, for a linear compressor, the volumetric efficiency depends not only on the mass flow rate but also the frequency, as seen in Equation (21). The piston stroke also varies slightly depending on the operating condition, which affects the volumetric efficiency. The overall isentropic efficiency is predicted by the model to within roughly 31% MAE as shown in Figure 13. MAE, mean absolute error, is defined as the average of the absolute value of errors.

The overall isentropic efficiency of the prototype compressor is significantly lower than

for typical commercially available compressors. However, the purpose of the prototype built in this work was merely to validate the model and not to obtain optimized performance. Since no commercial prototype was available which could be tested for this work, the compressor was made in-house, and could admittedly be significantly improved. However, the operating principles underlying the model and the prototype are identical, and therefore, the experiments serve the purpose of validating model predictions. It is expected that the model can form the basis for more optimized prototypes to be designed. The model developed in this work can be applied in the analysis of any linear compressor application.

The agreement with experiment of the value of the stroke predicted by the model is evidence that the vibration sub-model captures the dynamics of the compressor piston well. The mass flow rates show larger discrepancies which suggests that either the valve model or the leakage model need further improvement. In other compressor models these flow paths are modeled using semi-empirical models for good agreement with the performance of a particular compressor (Mathison et al., 2008, Kim and Groll, 2007, Navarro et al., 2007). The models presented here, in contrast, are based on first-principles in an effort to add flexibility to the model for use in parametric studies.

Additionally, the sensitivity to small changes in the values of the key parameters identified in this work (i.e. leakage gap, eccentricity, motor efficiency, and dry friction coefficient) may also explain errors. It was found that given a particular set of operating conditions, a 5% change in the value of eccentricity could lead to a 24% change in overall isentropic efficiency. Each of the identified parameters is difficult to quantify with a high degree of accuracy. Therefore, it can be concluded that there is potentially a significant amount of uncertainty due to the selection of these parameters which can explain a portion of the error in matching experimental data.

5. Conclusions

A comprehensive model of a miniature-scale linear compressor for electronics cooling applications is developed. The model consists of a vibration sub-model that is particular to the operation of a linear compressor as well as other sub-models for valve flow, leakage

past the piston, and heat transfer. The valve and leakage models are developed from first principles. The model is shown to predict the dynamic behavior of the piston well. Both the trends and quantitative values of the mass flow rate, volumetric, and overall isentropic efficiencies, respectively, are also predicted to within reasonable bounds.

Sensitivity to specific model parameters is critical to the overall performance of the compressor. These parameters should be further investigated in an effort to determine an optimum design for electronics cooling. Starting with a desired operating condition, the model can be used to optimize the compressor stroke, cylinder diameter and leakage gap. In addition, the model can be used to determine the correct mechanical spring rate and required motor power which are used to estimate overall package size.

6. Acknowledgment

Cadman, R., Cohen, R., 1969a. Electrodynamic oscillating compressors: Part 1 design based on linearized loads. ASME J. Basic Eng December, 656–663.

Cadman, R., Cohen, R., 1969b. Electrodynamic oscillating compressors: Part 2 evaluation of specific designs for gas load. ASME J. Basic Eng. December, 664–670.

Chen, Y., Halm, N. P., Braun, J. E., Groll, E. A., 2002a. Mathematical modeling of scroll compressors - part ii: Overall scroll compressor modeling. International Journal of Refrigeration 25 (6), 751–764.

Chen, Y., Halm, N. P., Groll, E. A., Braun, J. E., 2002b. Mathematical modeling of scroll compressors - part i: Compression process modeling. International Journal of Refrigeration 25 (6), 731–750.

Chiriac, V., Chiriac, F., 2008. An overview and comparison of various refrigeration methods for microelectronics cooling. In: Thermal and Thermomechanical Phenomena in Electronic Systems, 2008. ITHERM 2008. 11th Intersociety conference on. pp. 618–625.

Cremaschi, L., Groll, E. A., Garimella, S. V., 2007. Performance potential and challenges of future refrigeration-based electronics cooling approaches. In: THERMES 2007: Thermal Challenges in Next Generation Electronic Systems. pp. 119–128.

Fagotti, F., Prata, A., 1998. A new correlation for instantaneous heat transfer between gas and cylinder in reciprocating compressors. In: Proceedings of the International Compressor Engineering Conference, Purdue University, West Lafayette, IN, USA. pp. 871–876.

Fox, R., McDonald, A., Pritchard, P., 2004. Introduction to Fluid Mechanics, 6th Edition. John Wiley and Sons.

Heydari, A., 2002. Miniature vapor compression refrigeration systems for active cooling of high performance computers. In: Thermal and Thermomechanical Phenomena in Electronic Systems, 2002. ITHERM 2002. The Eighth Intersociety Conference on. pp. 371–378.

Hilpert, R., 1933. Wärmeabgabe von geheizten Drähten und Rohren im Luftstrom (Heat transfer from heated wires and pipes in the air). Forsch. Geb. Ingenieurwes. 4, 215.

Hubacher, B., Groll, E., Hoffinger, C., 2002. Performance measurements of a semi-hermetic carbon dioxide compressor. In: Proceedings of the International Refrigeration and Air Conditioning Conference, Purdue University, West Lafayette, IN USA. No. R11-10.

Kim, H., Roh, C.-g., Kim, J.-k., Shin, J.-m., Hwang, Y., Lee, J.-k., 2009. An experimental and numerical study on dynamic characteristic of linear compressor in refrigeration system. International Journal of Refrigeration 32 (7), 1536–1543.

Kim, J., Groll, E., 2007. Feasibility study of a bowtie compressor with novel capacity modulation. International Journal of Refrigeration 30 (8), 1427–1438.

Lee, H., Heo, J., Song, G., Park, K., Hyeon, S., Jeon, Y., 2001. Loss analysis of linear compressor. In: Compressors and their Systems: 7th International Conference. p. 305.

Lee, H., Jeong, S., Lee, C., Lee, H., 2004. Linear compressor for air-conditioner. In: Proceedings of the International Compressor Engineering Conference, Purdue University, West Lafayette, IN, USA. No. C047.

Mathison, M. M., Braun, J. E., Groll, E. A., 2008. Modeling of a two-stage rotary compressor. HVAC&R Research 14 (5), 719–748.

Mongia, R., Masahiro, K., DiStefano, E., Barry, J., Chen, W., Izenson, M., Possamai, F., Zimmermann, A., Mochizuki, M., 2006. Small scale refrigeration system for electronics cooling within a notebook computer. In: Thermal and Thermomechanical Phenomena in Electronics Systems, 2006. ITHERM'06. The Tenth Intersociety Conference on. pp. 751–758.

Moran, M., Shapiro, H., 2004. Fundamentals of Engineering Thermodynamics, 5th Edition. John Wiley and Sons.

Navarro, E., Granryd, E., Urchueguia, J. F., Corberan, J. M., 2007. A phenomenological model for analyzing reciprocating compressors. International Journal of Refrigeration 30 (7), 1254–1265.

Pollak, E., Soedel, W., Cohen, R., Friedlaender, F., 1979. On the resonance and operational behavior of an oscillating electrodynamic compressor. Journal of Sound and Vibration 67, 121–133.

Possamai, F., D.E.B., L., Zummermann, A., Mongia, R., 2008. Miniature vapor compression system. In: Proceedings of the International Compressor Engineering Conference, Purdue University, West Lafayette, IN, USA. No. 2932.

Rao, S. S., 2004. Mechanical Vibrations, 4th Edition. Prentice Hall.

Sathe, A., Groll, E., Garimella, S., 2008. Experimental evaluation of a miniature rotary compressor for application in electronics cooling. In: Proceedings of the International Compressor Engineering Conference, Purdue University, West Lafayette, IN, USA. No. 1115.

Tillner-Roth, R., Baehr, H., 1994. An international standard formulation for the thermodynamic properties of 1, 1, 1, 2-tetrafluoroethane (hfc-134a) for temperatures from 170 k to 455 k and pressures up to 70 mpa. Journal of Physical and Chemical Reference Data 23, 657.

Trutassanawin, S., Groll, E. A., Garimella, S. V., Cremaschi, L., 2006. Experimental investigation of a miniature-scale refrigeration system for electronics cooling. IEEE Transactions on Components and Packaging Technologies 29 (3), 678.

Unger, R., 1998. Linear compressors for clean and specialty gases. In: Proceedings of the International Compressor Engineering Conference, Purdue University, West Lafayette, IN, USA. Vol. 1. p. 51.

Unger, R., Novotny, S., 2002. A high performance linear compressor for cpu cooling. In: Proceedings of the International Compressor Engineering Conference, Purdue University, West Lafayette, IN, USA. No. C23-3.

Van der Walt, N., Unger, R., 1994. Linear compressors-a maturing technology. In: Proceedings of the International Compressor Engineering Conference, Purdue University, West Lafayette, IN, USA. pp. 239–246.

List of Tables

Table 1: Linear compressor prototype parameters.

k_{mech}	f	A_p	g	η_{motor}	ϵ	$V_{cyl,max}$
$N\ m^{-1}$	–	cm^2	mm	–	cm	cm^3
23000	0.35	1.217	0.37	0.417	1.145	3.091

Table 2: Summary of experimental data.

P_{suc}	T_{suc}	P_{dis}	T_{dis}	x_p	$\dot{m}$	f	$\dot{W}_{in}$	η_{vol}	$\eta_{o,is}$
kPa	K	kPa	K	cm	$g\ s^{-1}$	Hz	W	–	–
557	296.8	641	300.4	0.5784	0.335	44.1	24.7	0.405	0.057
561	297.0	702	299.8	0.5756	0.143	44.1	24.0	0.173	0.040
559	298.1	709	301.1	0.5951	0.120	44.1	23.6	0.141	0.028
534	295.4	587	300.3	0.6445	0.461	44.6	17.5	0.505	0.037
537	295.3	619	300.6	0.6695	0.380	44.6	17.1	0.398	0.048
537	295.3	651	300.2	0.6682	0.267	44.6	22.0	0.280	0.046

List of Figures

Figure 1: Pressure over enthalpy diagram of typical R134a miniature-scale refrigeration cycle for electronics cooling.
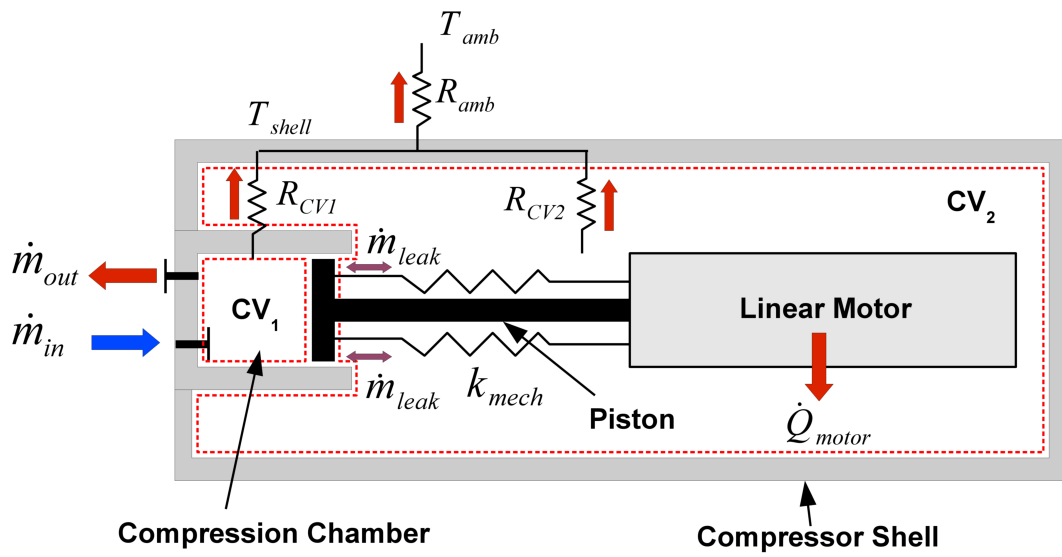
Figure 2: Representation of the compression process in a linear compressor.
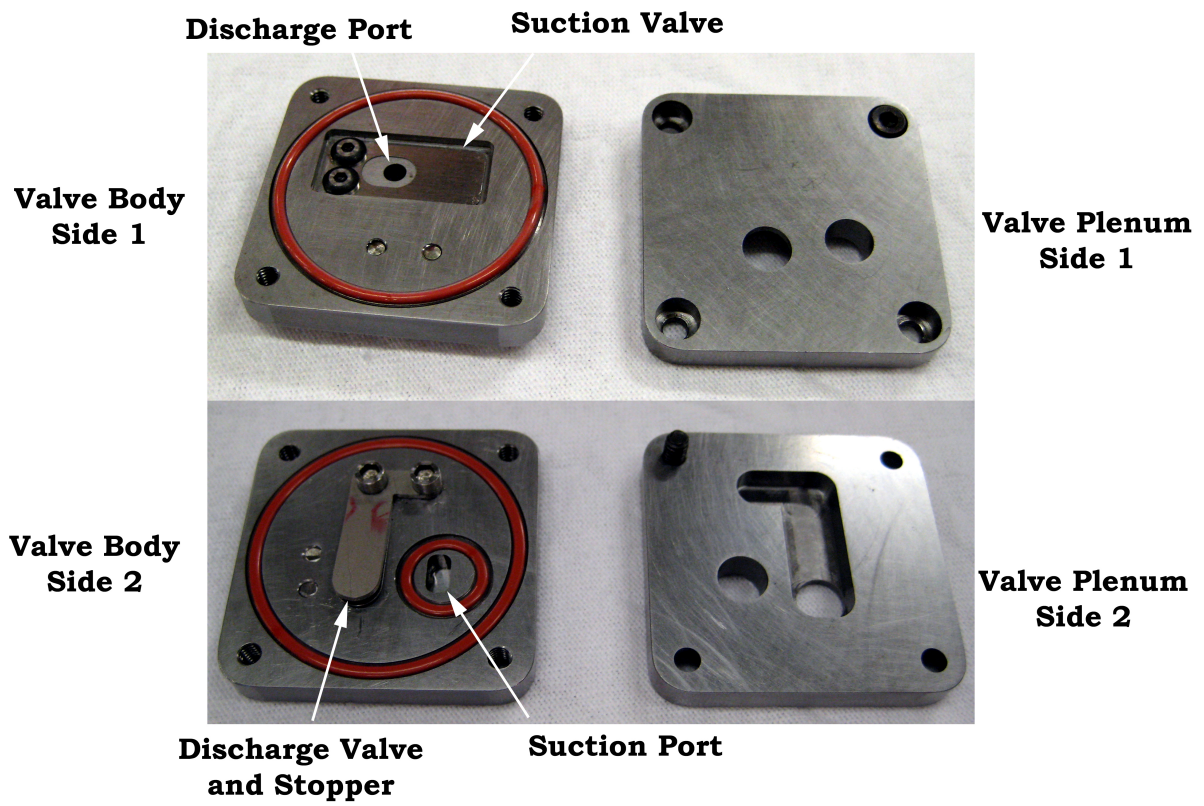
Figure 3: Photos of reed valve assembly used in compressor prototype.
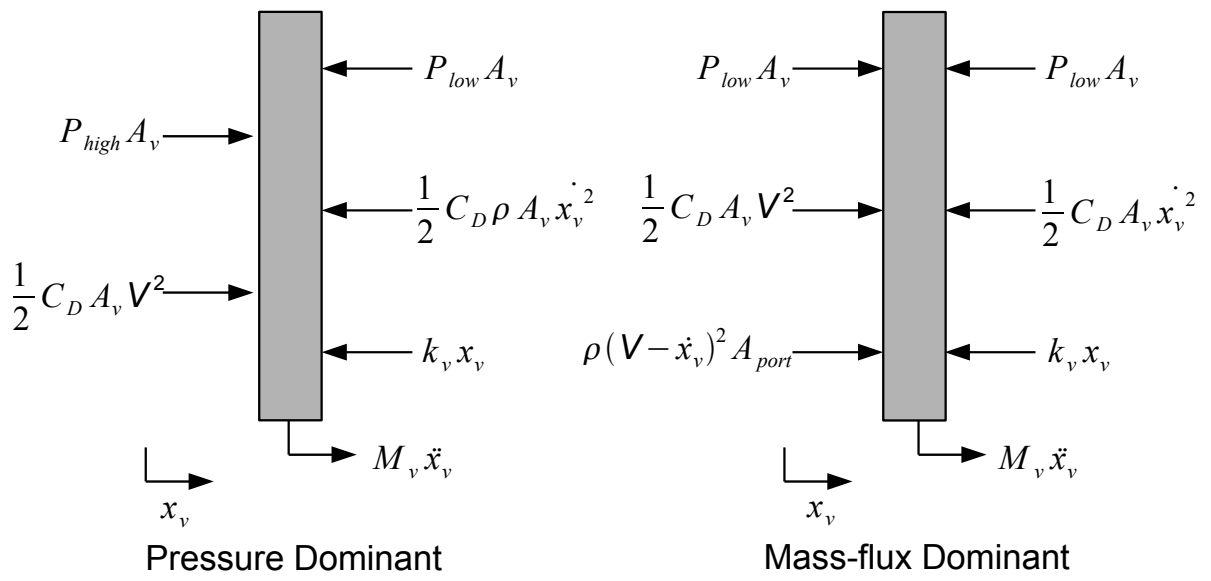
Figure 4: Free body diagrams for the valve reed.
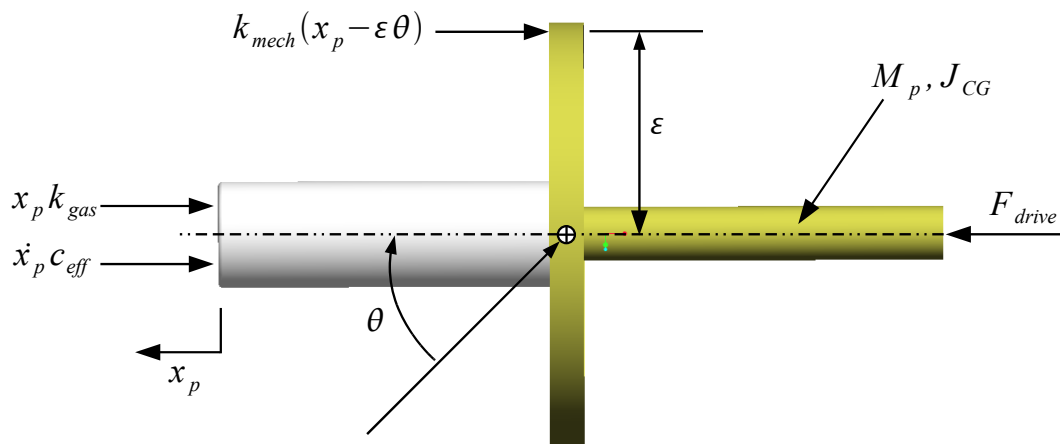
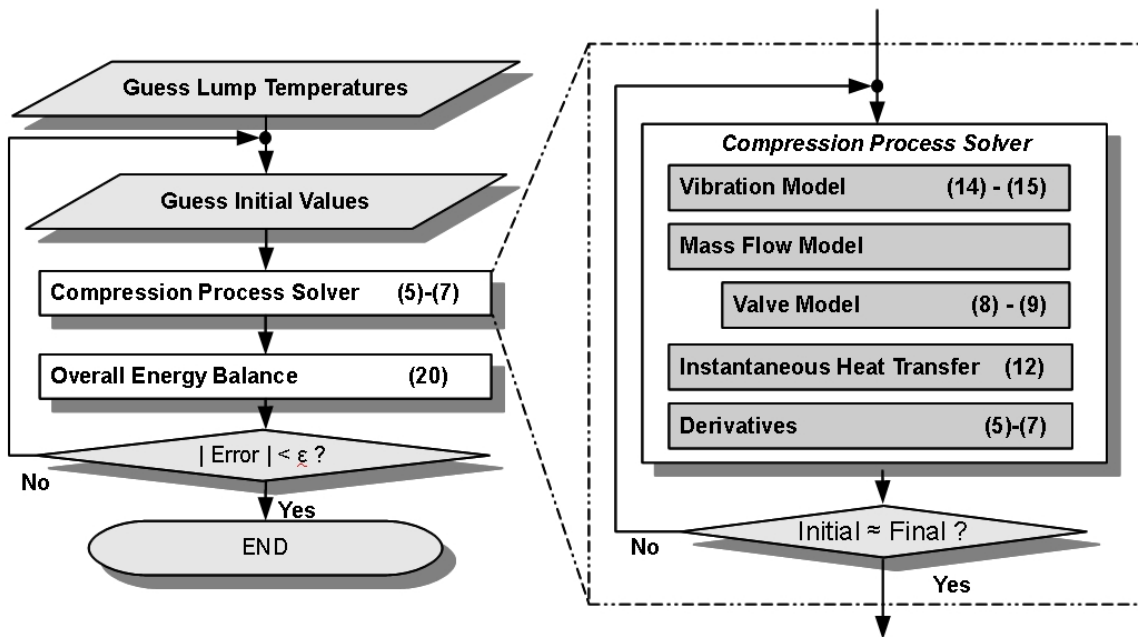Figure 5: Free body diagram of linear compressor piston assembly.

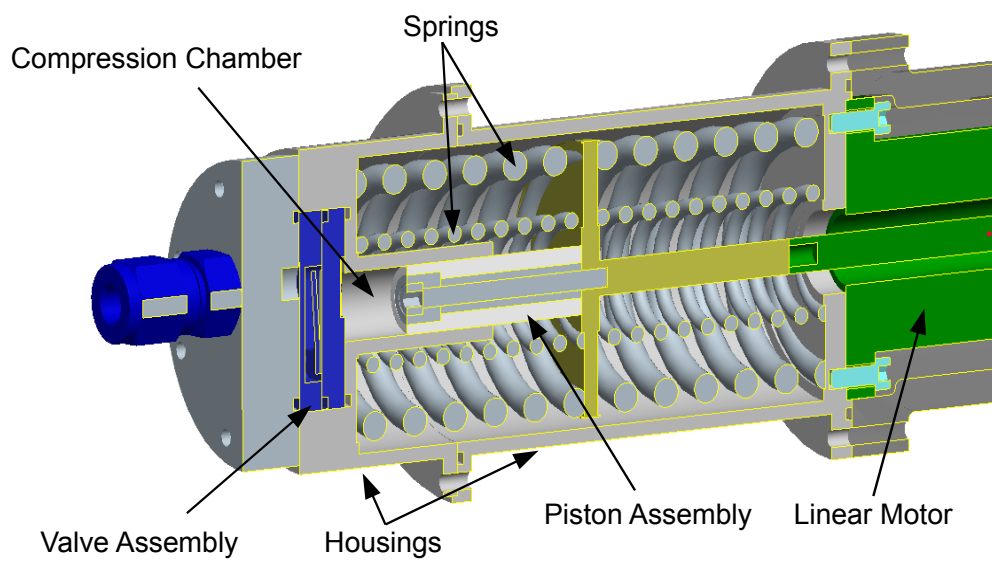Figure 6: Solution flowchart of linear compressor model (equations solved at each step given in blocks).

Figure 7: A section view of the prototype linear compressor.
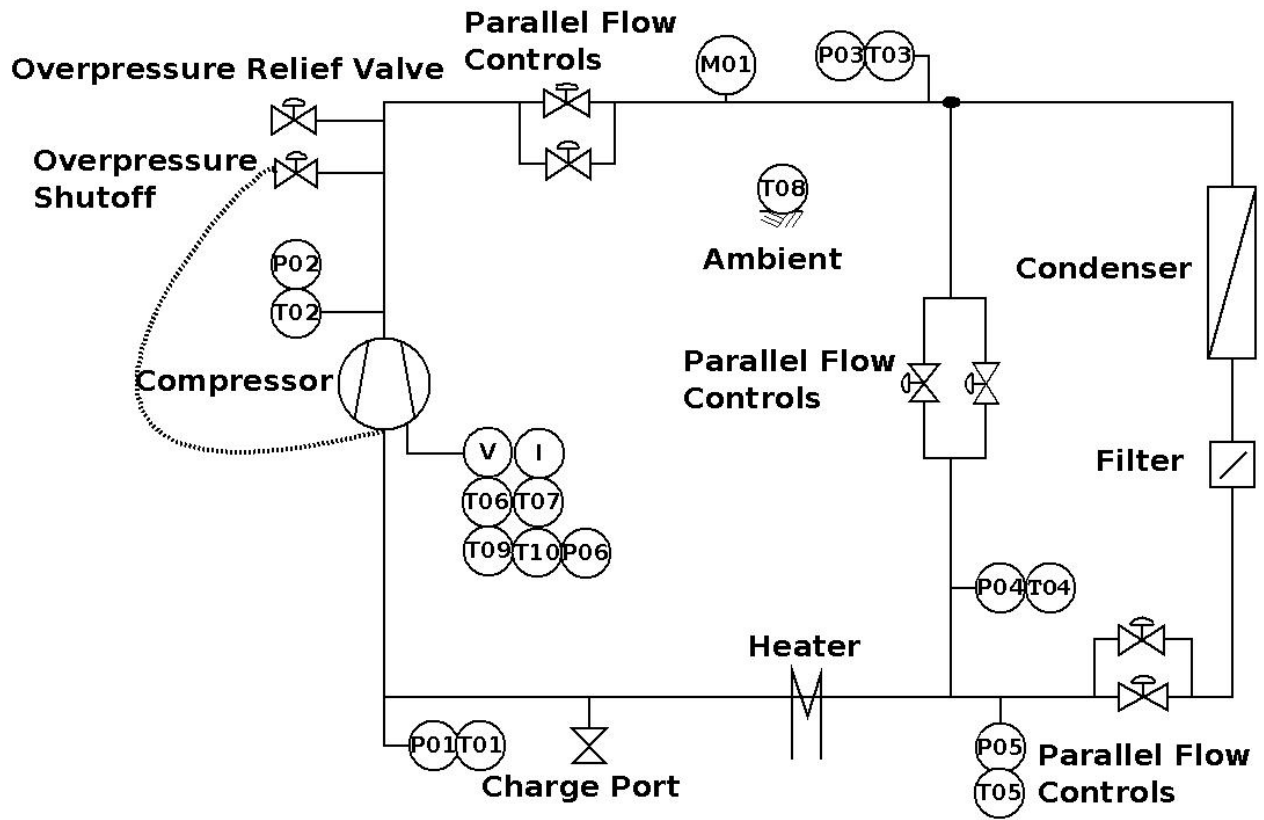
Figure 8: Schematic diagram of miniature-compressor hot gas bypass load stand.
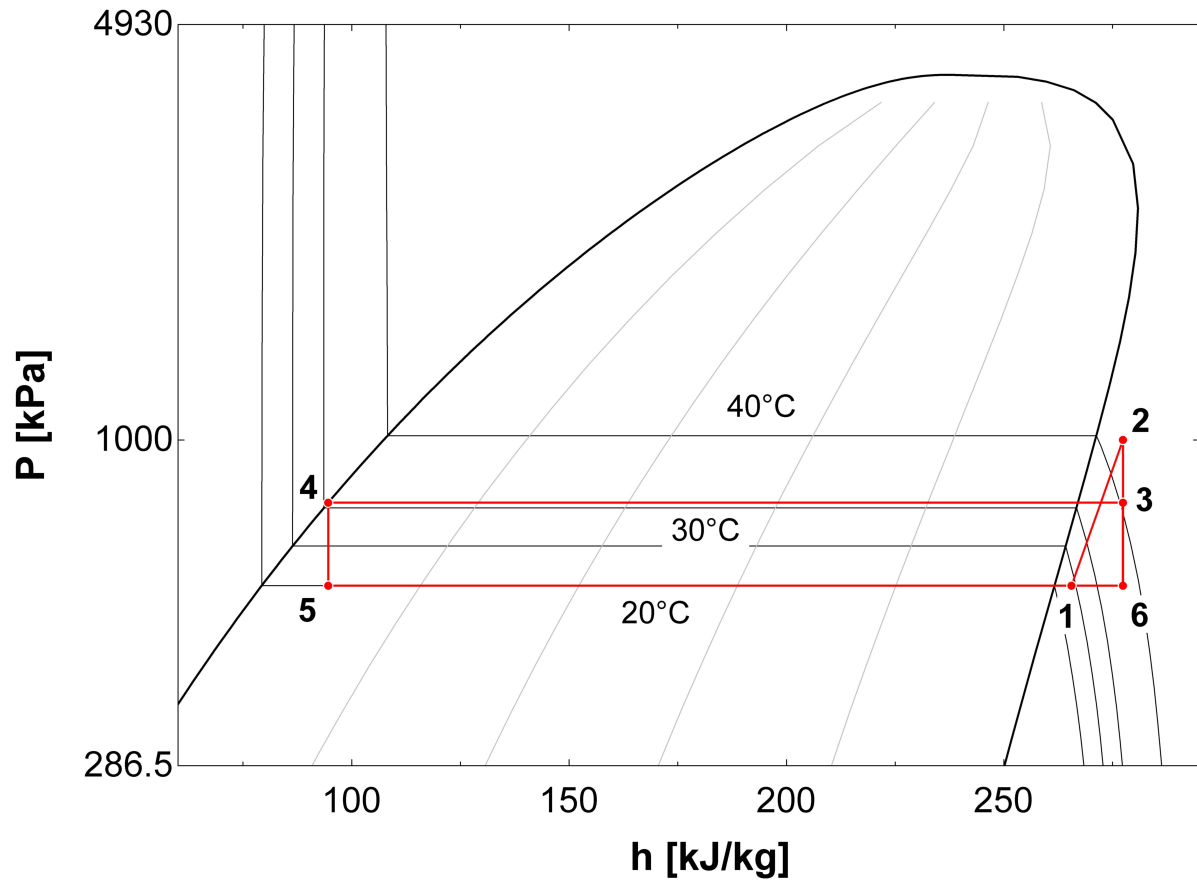
Figure 9: Pressure enthalpy plot of compressor load stand operation.
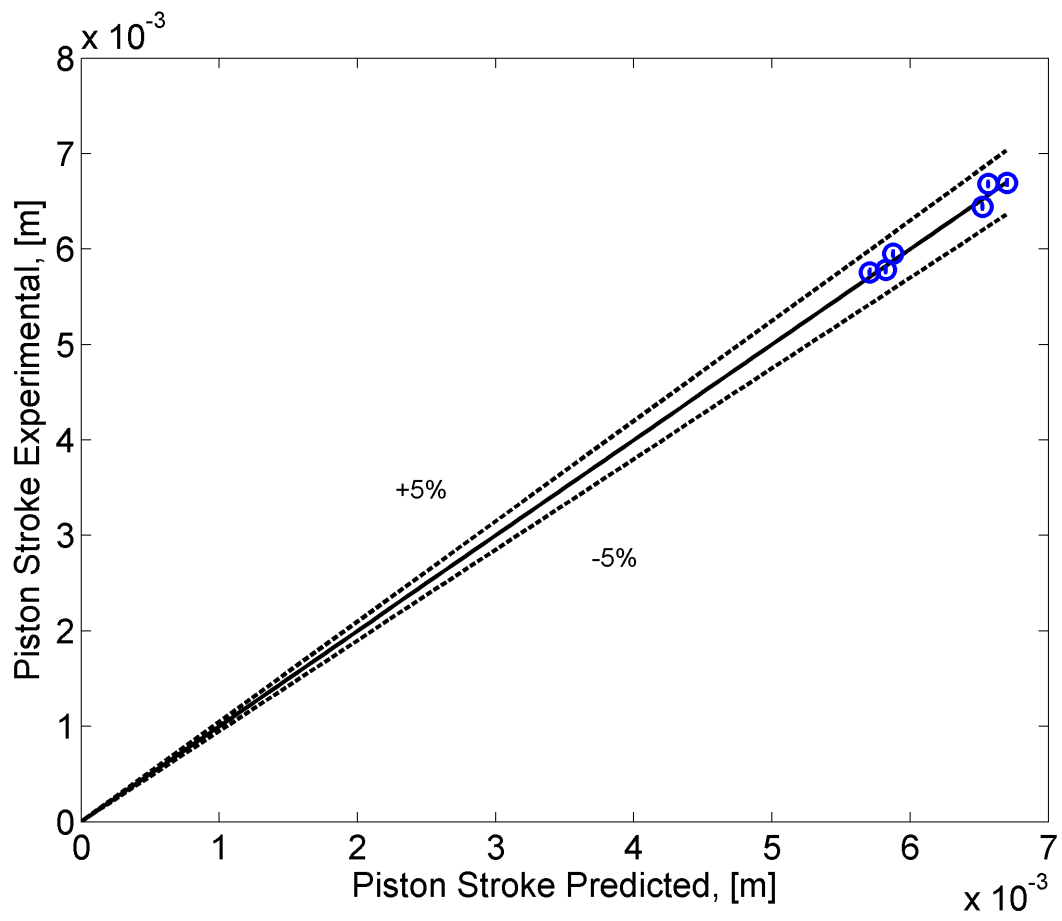
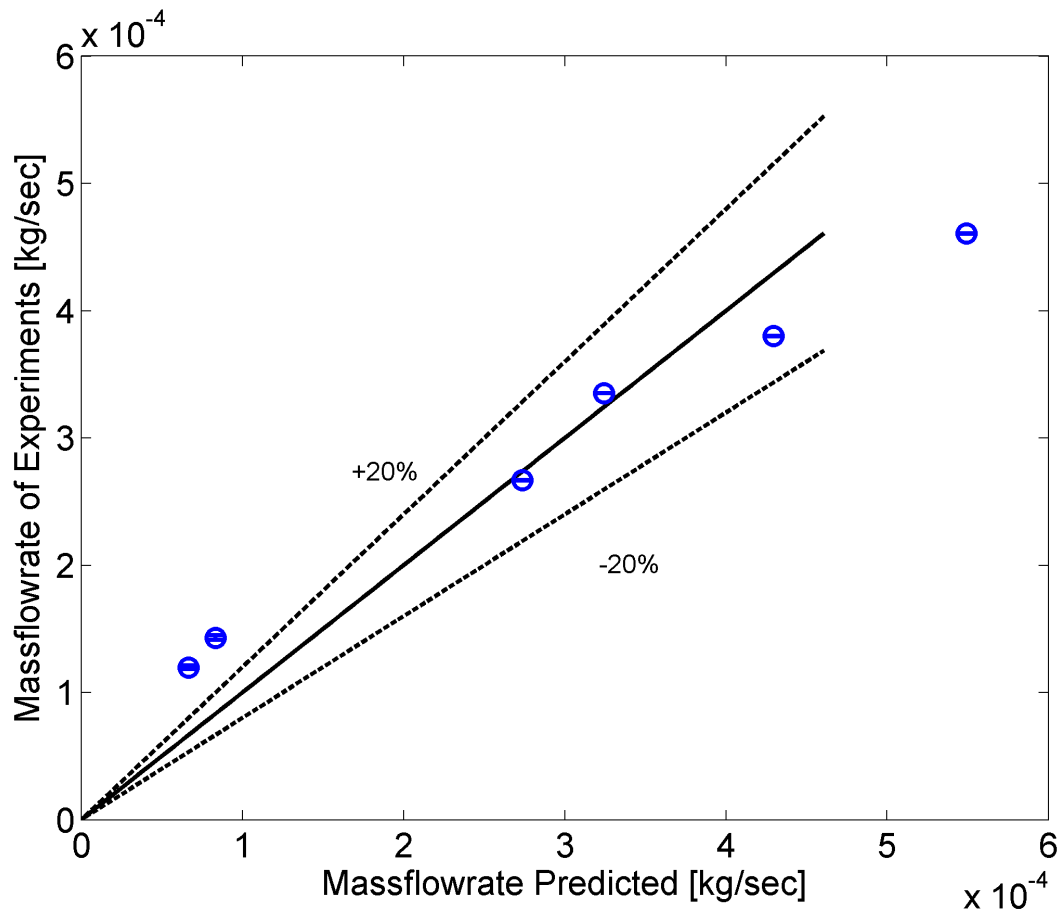Figure 10: Comparison of experimental and predicted piston displacements.

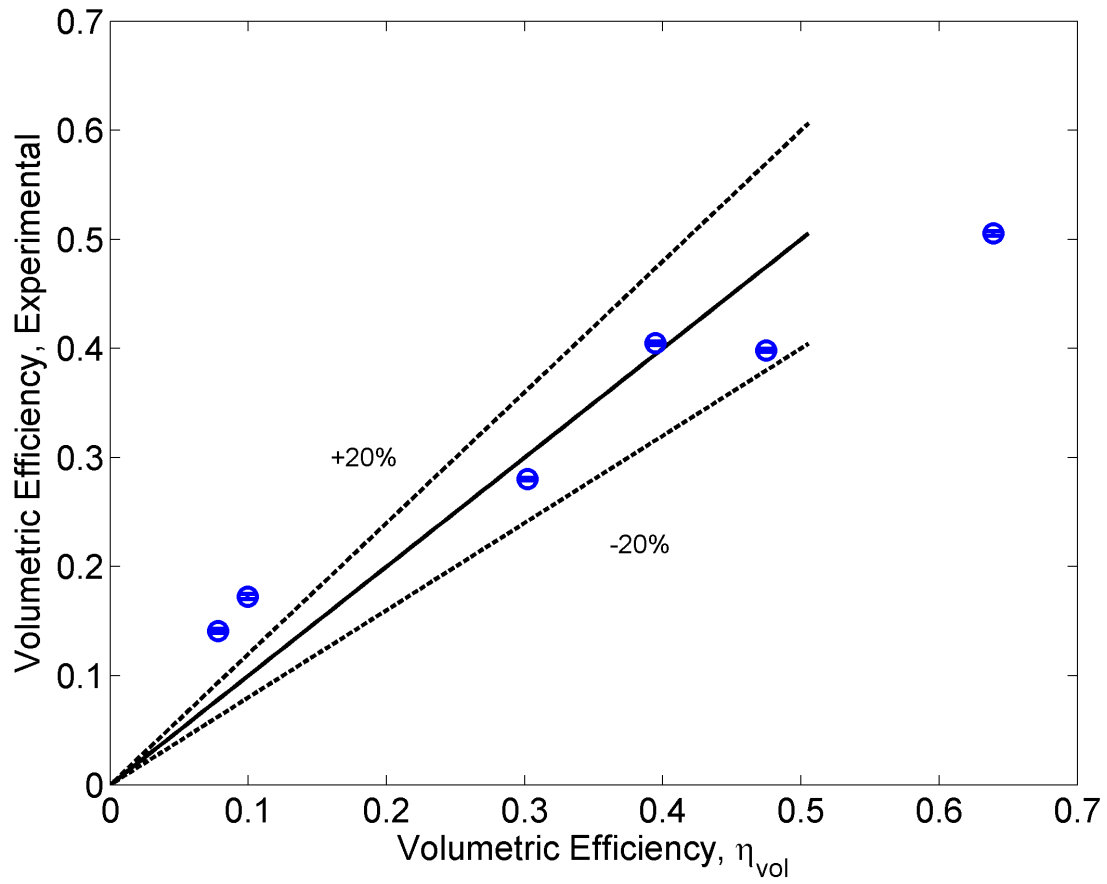Figure 11: Comparison of experimental and predicted mass flow rates.

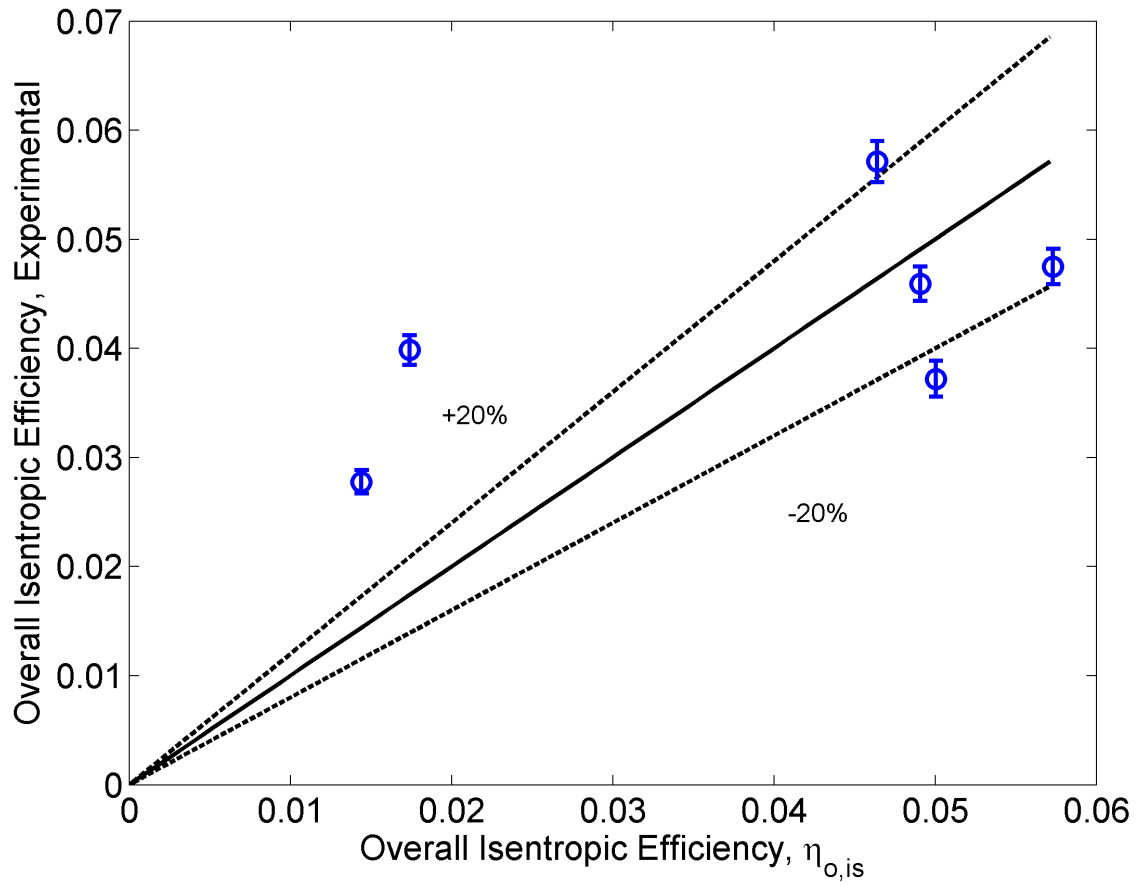Figure 12: Comparison of experimental and predicted volumetric efficiencies.

Figure 13: Comparison of experimental and predicted overall isentropic efficiencies.